Proceedings of the ASME 2022
International Mechanical Engineering Congress and Exposition
IMECE2022
October 30-November 3, 2022, Columbus, Ohio, USA

IMECE2022-95630

PHONON BOLTZMANN TRANSPORT EQUATION BASED SIMULATION OF FREQUENCY DOMAIN THERMOREFLECTANCE EXPERIMENTS

SIDDHARTH SAURAV
SANDIP MAZUMDER*
Department of Mechanical and Aerospace Engineering
The Ohio State University, Columbus, OH 43210, USA

ABSTRACT

The Boltzmann Transport equation (BTE) was solved numerically in cylindrical coordinates and in time domain to simulate a Frequency Domain Thermo-Reflectance (FDTR) experiment. First, a parallel phonon BTE solver that accounts for all phonon modes, frequencies, and polarizations was developed and tested. The solver employs the finite-volume method (FVM) for discretization of physical space, and the finite-angle method (FAM) for discretization of angular space. The solution was advanced in time using explicit time marching. The simulations were carried out in time domain and band-based parallelization of the BTE solver was implemented. The phase lag between the temperature averaged over the probed region of the transducer and the modulated laser pump signal was extracted for a pump laser modulation frequency ranging from 20-200 MHz. It was found that with the relaxation time scales used in the present study, the computed phase lag is underpredicted when compared to experimental data, especially at smaller modulation frequencies. The challenges in solving the BTE for such applications are highlighted.

NOMENCLATURE

A	area [m^2]
c	specific heat capacity per unit volume [J m^{-3} K^{-1}]
D	density of states per unit volume [m^{-3}]
f	number density function
f_0	equilibrium number density function
$G_{\omega,p}$	spectral directionally integrated intensity [Wm^{-2} $rad^{-1}s$]
G_C	contact conductance [W m^{-2} K^{-1}]
$\hbar$	Dirac constant = 1.0546 x 10^{-34} [$m^2kg.s^{-1}$]
$I_{\omega,p}$	spectral directional phonon intensity [$Wm^{-2}sr^{-1}rad^{-1}s$]
$I_{0,\omega,p}$	equilibrium phonon intensity [$Wm^{-2}sr^{-1}rad^{-1}s$]
k_B	Boltzmann constant = 1.381 x 10^{-23} [$m^2kg.s^{-2}K^{-1}$]
k_T	thermal conductivity of transducer [W m^{-1} K^{-1}]
$\hat{\mathbf{n}}$	unit surface normal vector
N_{band}	total number of spectral intervals (or bands)
N_{dir}	number of solid angles (or directions)
p	phonon polarization index
$\mathbf{q}$	heat flux vector [Wm^{-2}]
$\dot{Q}$	heat transfer rate [W]
r	radial coordinate or radius [m]
$\mathbf{r}$	position vector [m]
$\hat{\mathbf{s}}$	unit direction vector
t	time [s]
T	absolute temperature [K]
V	volume of cell [m^3]
z	axial coordinate or thickness [m]

Greek

ρ_T	density of transducer [kg m^{-3}]
θ	polar angle [radians]
$\boldsymbol{\upsilon}_{\omega,p}$	phonon group velocity vector [m s^{-1}]
$\tau_{\omega,p}$	spectral relaxation time scale [s]
ω	angular frequency [rad s^{-1}]
ω_L	modulation frequency of pump laser [Hz]
Ω	solid angle (sr)
ψ	azimuthal angle [rad]

INTRODUCTION

Frequency Domain Thermo-Reflectance (FDTR) is a commonly used noncontact optical pump probe technique based on thermo-reflectance for the study of heat transport at small time and length scales, i.e., at scales comparable to or smaller than the

*E-mail: mazumder.2@osu.edu, Fellow ASME

mean free paths of the energy-carrying phonons. In FDTR, the sample, which is covered by a thin metallic layer called the *transducer*, is heated using a modulated continuous wave pump laser beam resulting in surface temperature (reflectivity) oscillations, which are then monitored using a probe laser. The lag in phase between the pump and probe laser signals is recorded. Extraction of the thermal conductivity of the substrate from the measured phase lag data requires use of a thermal transport model.

The most common model used for this purpose is based on the solution of the Fourier heat conduction equation in frequency domain. This was brought to the limelight by Cahill [1] and has been used by the vast majority of researchers since then [2,3]. The presence of a transducer makes it a multiple layer problem which is treated using the Feldman algorithm [4]. Interfaces between layers are treated as artificial layers whose thermal properties are adjusted to reproduce measured interface conductance values. Unfortunately, these closed-form analytical models are unable to make a distinction between changes made to the pump laser spot size (diameter) versus the probe laser spot size [5]. The problem may be overcome by resorting to numerical solution of the Fourier heat conduction equation [5].

The thermal conductivity extracted from FDTR experiments using such a Fourier law-based model has been found to change when the modulation frequency of the pump laser is changed [1-3,6]. The Fourier law assumes that all phonons travel with infinite velocity resulting in very small mean free paths. The dependence of thermal conductivity on the modulation frequency is attributed to the fact that when the laser modulation frequency is high, the thermal penetration depth, which is inversely proportional to the square root of the modulation frequency, is small, and can often be smaller than the mean free path of some of the energy-carrying phonons. As a result, some phonons hardly scatter. This results in so-called ballistic-diffusive transport or quasi-ballistic transport. In this regime of transport, the effective thermal conductivity has been found to be smaller than the bulk value—a phenomenon known as thermal conductivity suppression [6-8].

Various enhancements to Fourier law-based models have been proposed in an effort to the capture the ballistic effects and predict the thermal conductivity suppression for different modulation frequencies. One class of these models [9] makes use of the hyperbolic heat conduction equation which accounts for a finite velocity for the phonons by introducing relaxation time as a parameter. However, all phonons are assumed to have the same velocity irrespective of their type and frequency. Two parameter models [10] have been used to treat the diffuse and ballistic phonons differently by introducing an additional term in the Fourier heat conduction equation that involves the characteristic ballistic heat transport length as an additional parameter. Higher-order correction terms from the BTE have been added to the Fourier law models for the treatment of ballistic phonons. Ramu and Bowers [11] proposed a two-band model in which a cut-off frequency is used to classify the phonons into ballistic and diffusive phonons. The ballistic phonons are then treated by adding a higher order correction term to the Fourier law that is derived from the phonon BTE. In a similar ballistic-diffusive model proposed by Chen [12], and later expanded to complex three-dimensional geometry by Mittal and Mazumder [13], the phonon intensity is split into a diffusive component and a ballistic component. More recently, a model that introduces a hydrodynamic term in the Fourier heat conduction equation—analogous to the advective term in the Navier-Stokes equation—has been proposed to capture ballistic effects [14].

The aforementioned approximate models have been used to avoid solving the full-fledged phonon BTE, as it is very challenging and time consuming to solve [15]. Peraud and Hadjiconstantinou [16] performed Monte Carlo simulations of phonon transport by using an energy-based deviational formulation. Regner et al. [17] solved the 1D BTE in frequency domain to extract the thermal conductivity accumulation and suppression functions. However, the influence of multidimensional thermal transport can only be captured by solving the multidimensional BTE. Ding et al. [18] used Monte Carlo study to simulate a single laser pulse of a TDTR experiment to demonstrate in-plane and cross-plane thermal conductivity suppression. Ali et al. [19] solved the full multidimensional phonon BTE for TDTR experiments in a 2D planar setup and the model demonstrated thermal conductivity suppression and its dependence on the modulation frequency of the pump laser without the use of any additional parameters.

The current work attempts to solve the BTE in a 2D axisymmetric domain (as opposed to 2D planar [19]). This is the first work of its kind where the solution in time domain is advanced to a point where the solution becomes quasi-periodic, enabling reliable extraction of the phase lag. This is in contrast with previous studies [16,18] that only simulated a single laser pulse. The present BTE solver uses the cylindrical coordinate system and accounts for all phonon modes, frequencies and polarization. It represents the first step toward extracting the thermal conductivity from FDTR experiments.

THEORY AND MATHEMATICAL MODEL

The Phonon Boltzmann Transport Equation (BTE)

The BTE can be used to model phonon transport in semi-conductors as phonons follow Bose-Einstein statistics and interact with each other via scattering events. The phonon BTE, under the single time scale approximation can be written as [9, 15]

$$\frac{\partial f}{\partial t} + \mathbf{v} \bullet \nabla f = \frac{f_0 - f}{\tau}, \tag{1}$$

where f is the distribution function of an ensemble of phonons, f_0 is the equilibrium number density function, τ is the scattering time scale and $\mathbf{v}$ is the phonon group velocity. The distribution function, f, for each polarization p, is a function of seven independent variables, i.e., $f = f(t, \mathbf{r}, \hat{\mathbf{s}}, \omega, p)$, where the unit direction vector, $\hat{\mathbf{s}}$, may be expressed in terms of the azimuthal angle, ψ, and polar angle, θ, as [20]

$$\hat{\mathbf{s}} = \sin\theta\cos\psi\,\hat{\mathbf{i}} + \sin\theta\sin\psi\,\hat{\mathbf{j}} + \cos\theta\,\hat{\mathbf{k}}. \tag{2}$$

If the Cartesian coordinate system is used to describe space, for example, one may write the functional dependence of f as $f = f(t, x, y, z, \theta, \psi, \omega, p)$. In other words, for a three-dimensional (3D) geometry, f is a function of 8 independent variables. Since polarizations are discrete, it is customary to

*E-mail: mazumder.2@osu.edu, Fellow ASME

think of f as being a function of 7 independent variables, with the implicit understanding that it is different for different polarizations. The group velocity is also dependent on direction: $\mathbf{v} = \mathbf{v}(\hat{\mathbf{s}}, \omega, p)$. The equilibrium Bose-Einstein distribution, on the other hand, is direction independent: $f_0 = f_0(\omega, T)$, as is the relaxation time-scale: $\tau = \tau(\omega, T, p)$. Following the seminal work of Majumdar [21], a phonon intensity may be defined in terms of the distribution function:

$$\begin{aligned} I_{\omega,p} &= I(t,\mathbf{r},\hat{\mathbf{s}},\omega,p) = \left|\mathbf{v}_{\omega,p}\right| \hbar\omega f \; D(\omega,p)/4\pi \\ I_{0,\omega,p} &= I_0(t,\mathbf{r},\omega,p) = \left|\mathbf{v}_{\omega,p}\right| \hbar\omega f_0 \; D(\omega,p)/4\pi \end{aligned}, \tag{3}$$

where $D(\omega, p)$ is the density of states, and $I_{\omega,p}$ is the spectral directional phonon intensity, while $I_{0,\omega,p}$ is the equilibrium spectral phonon intensity. Substitution of Eq. (3) into Eq. (1) yields [21]

$$\frac{\partial I_{\omega,p}}{\partial t} + \mathbf{v}_{\omega,p} \bullet \nabla I_{\omega,p} = \frac{I_{0,\omega,p} - I_{\omega,p}}{\tau_{\omega,p}}. \tag{4}$$

For any given frequency and polarization, the intensity, $I_{\omega,p}$, is a function of time, 3 space variables (in 3D), and 2 directional variables, making Eq. (4) a six-dimensional equation. Furthermore, it needs to be solved for all frequency and polarizations in order to determine the heat flux, as is discussed in the sub-section to follow.

Solution of the BTE [Eq. (4)] necessitates boundary conditions for the intensity. Two types of boundary conditions are generally used: (1) thermalizing, and (2) reflective. At a thermalizing boundary, phonons are emitted from it based on the equilibrium energy distribution and any phonon that strikes it immediately gets absorbed. The boundary condition is mathematically written as $I_{\omega,p} = I_{0,\omega,p}$, where $\mathbf{r}_w$ is the position vector of the boundary or wall, and $\hat{\mathbf{s}}_o$ is the outgoing direction for the intensity. In an axisymmetric domain, the treatment of the axis of symmetry requires special numerical treatment, and this is discussed in a later section.

Heat Flux and Energy Conservation (First Law)

Once the BTE [Eq. (4)] has been solved, the heat flux may be calculated from the phonon intensity using the relationship [15,20]

$$\begin{aligned} \mathbf{q}(t,\mathbf{r}) &= \sum_p \int_{\omega_{\min,p}}^{\omega_{\max,p}} \int_{4\pi} I_{\omega,p}(t,\mathbf{r},\hat{\mathbf{s}},\omega,p)\,\hat{\mathbf{s}}\,d\Omega\,d\omega \\ &= \sum_p \int_{\omega_{\min,p}}^{\omega_{\max,p}} \mathbf{q}_{\omega,p}(t,\mathbf{r})\,d\omega \end{aligned}, \tag{5}$$

where the integrals are over all solid angles Ω and the frequency range of each polarization; $\omega_{\max,p}$ and $\omega_{\min,p}$ are the maximum and minimum frequencies, respectively, corresponding to a given polarization, p. In Eq. (5), $\mathbf{q}_{\omega,p}$ denotes the spectral heat flux while $\mathbf{q}$ denotes the total heat flux. Substitution of Eqs. (4) and (5) into the energy conservation equation (First Law), followed by some manipulation, yields [15]:

$$\begin{aligned} &\frac{\partial}{\partial t}\left(\sum_p \int_{\omega_{\min,p}}^{\omega_{\max,p}} \frac{\hbar\omega D(\omega,p)}{\exp[\hbar\omega/k_B T]-1} d\omega\right) = \\ &-\sum_p \int_{\omega_{\min,p}}^{\omega_{\max,p}} \frac{1}{\left|\mathbf{v}_{\omega,p}\right|}\left[\frac{1}{\tau_{\omega,p}}\left(\frac{\left|\mathbf{v}_{\omega,p}\right|\hbar\omega D(\omega,p)}{\exp[\hbar\omega/k_B T]-1} - G_{\omega,p}\right) - \frac{\partial G_{\omega,p}}{\partial t}\right] d\omega \end{aligned} \tag{6}$$

where

$$G_{\omega,p} = \int_{4\pi} I_{\omega,p}\, d\Omega. \tag{7}$$

Equation (6) is a nonlinear equation that may be solved to obtain the so-called pseudo-temperature [15,22] at any location within the computational domain. In the section to follow, numerical techniques for solution of the BTE are discussed.

NUMERICAL SOLUTION

The present work uses the finite angle method [15,20] for solving the BTE [Eq. (4)]. It is discussed next, along with treatment of the axis of symmetry and the transducer, which is a metallic film that covers the substrate.

Finite Angle Method (FAM)

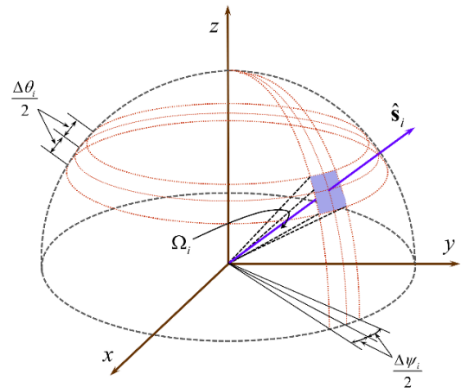

Figure 1: Polar coordinate system used for angular discretization in the FAM.

The FAM is a variant of the discrete ordinates method [20]. In the FAM, the entire solid angle space is first split into a set of nonoverlapping smaller solid angles. These smaller solid angles may be based equal subdivisions in θ and ψ, as shown in Fig. 1. The BTE [Eq. (4)] is first integrated over a volume [finite volume method in space on a structured mesh with cell index (j,k)], followed by finite solid angles to yield [15,20]:

$$\begin{aligned} &\left.\frac{\partial I_{i,\omega,p}}{\partial t}\right|_k V_{j,k}\Omega_i + \left|\mathbf{v}_{\omega,p}\right| \sum_{f=1}^{N_{f,k}} I_{i,\omega,p,f(j,k)}(\mathbf{S}_i \bullet \hat{\mathbf{n}}_f) A_{f,j,k} \\ &= \frac{1}{\tau_{\omega,p,j,k}}(I_{o,\omega,p,k} - I_{i,\omega,p,j,k}) V_k \Omega_i \quad \forall i = 1,2,...,N_{dir} \end{aligned}, \tag{8}$$

where $V_{j,k}$ is the volume of the k-th cell, $A_{f,j,k}$ is the area of the f-th face of the (j,k)-th cell, and

$$\begin{aligned} \Omega_i &= \int_{\Delta\Omega_i} d\Omega = \int_{\theta_i-\Delta\theta_i/2}^{\theta_i+\Delta\theta_i/2} \int_{\psi_i-\Delta\psi_i/2}^{\psi_i+\Delta\psi_i/2} \sin\theta\, d\theta\, d\psi \\ &= 2\sin\theta_i \sin\left(\frac{\Delta\psi_i}{2}\right)\Delta\psi_i \end{aligned}, \tag{9}$$

*E-mail: mazumder.2@osu.edu, Fellow ASME

and

$$\mathbf{S}_i = \cos\psi_i \sin\left(\frac{\Delta\psi_i}{2}\right)[\Delta\theta_i - \cos(2\theta_i)\sin(\Delta\theta_i)]\hat{\mathbf{i}} + \sin\psi_i \sin\left(\frac{\Delta\psi_i}{2}\right)[\Delta\theta_i - \cos(2\theta_i)\sin(\Delta\theta_i)]\hat{\mathbf{j}} + \left(\frac{\Delta\psi_i}{2}\right)\sin(2\theta_i)\sin(\Delta\theta_i)\hat{\mathbf{k}} \quad (10)$$

The subscript i for the intensity now denotes an intensity along a line of sight passing through the center of the solid angle, i.e., in the direction $\hat{\mathbf{s}}_i$ (see Fig. 1). Finally, the face intensity in Eq. (8) is expressed in terms of cell-center intensities using the first-order upwind scheme [15]:

$$I_{i,\omega,p,f(j,k)} = \begin{cases} I_{i,\omega,p,j,k} & \text{if } \hat{\mathbf{s}}_i \bullet \hat{\mathbf{n}}_f > 0 \\ I_{i,\omega,p,N(f)} & \text{if } \hat{\mathbf{s}}_i \bullet \hat{\mathbf{n}}_f < 0 \end{cases}, \quad (11)$$

where $N(f)$ denotes the neighboring cell next to face f, as shown in Fig. 2.

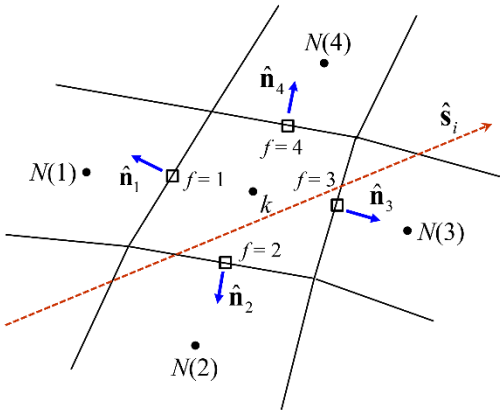

Figure 2: Schematic representation of geometric quantities used for finite volume discretization of the BTE.

As a final note, the cylindrical coordinates, the volume appearing in Eq. (8) can be determined using $V_{j,k} = \int_{z_b}^{z_t}\int_{r_i}^{r_o} 2\pi r dr\, dz$, where r_i and r_o are inner and outer radii, respectively, while z_b and z_t are bottom and top z-coordinates, respectively. For any horizontal face, the area is given by $A_{f,j,k} = \pi(r_o^2 - r_i^2)$, while for any vertical face, the area is given by $A_{f,j,k} = 2\pi r_o z_T$.

Treatment of the Transducer

The transducer is metallic. In this study, heat conduction in the transducer is treated using the Fourier law. Furthermore, since the transducer is very thin, it is assumed that there is no temperature variation within the transducer in the z direction (Fig. 3). The only variation is in the r direction. With this premise, the computational domain may be discretized using a structured mesh in the r-z plane, as shown in Fig. 4.

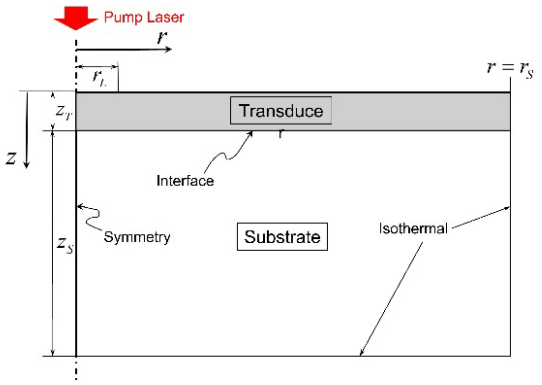

Figure 3: Two-dimensional axisymmetric representation of an FDTR setup.

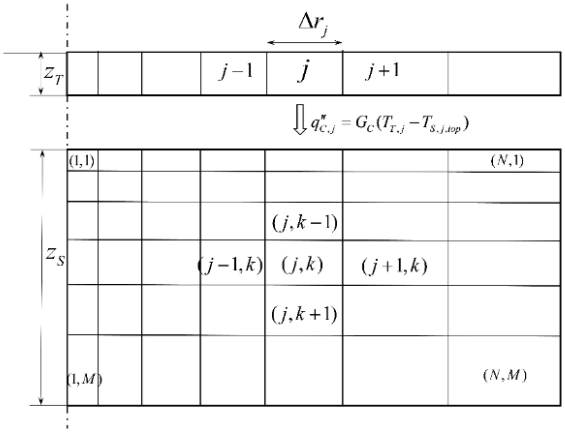

Figure 4: Structured mesh in the r-z plane used to discretize the substrate and the transducer.

The governing equation for heat transfer in the transducer may be derived from an energy balance, and is written as

$$\rho_T c_T \frac{\partial T_T}{\partial t} = \frac{k_T}{r}\frac{\partial}{\partial r}\left(r\frac{\partial T_T}{\partial r}\right) + \frac{(q_t'' - q_b'')}{z_T} \quad (12)$$

where ρ_T, c_T, k_T, and z_T are the density, specific heat capacity, thermal conductivity, and thickness of the transducer, respectively. The temperature of the transducer is given by T_T. The heat fluxes at the top and bottom surfaces of the transducer are denoted by q_t'' and q_b'', respectively. The heat flux on the top surface is the energy supplied by the pump laser, and is a known quantity, written as

$$q_t'' = q_L''(r)[1 + \sin\omega_L t] \quad (13)$$

where $q_L''(r)$ is the radially varying (such as Gaussian) laser flux, and ω_L is the modulation frequency of the pump laser. The heat flux on the bottom surface of the transducer is not a known quantity. However, it can be related to the substrate through the relationship

$$q_b'' = G_C(T_T - T_{top}) \quad (14)$$

where T_{top} is the temperature on the top of the substrate surface, and G_C is the contact conductance between the transducer and the substrate. Although T_{top} is not directly known, it can be derived from the solution (of temperature) in the substrate, which

*E-mail: mazumder.2@osu.edu, Fellow ASME

in turn, requires solution of the BTE. Thus, coupling the transducer to the substrate requires a self-consistent iterative procedure. This procedure is described in the section to follow.

As a final step, applying the finite-volume procedure [23] for discretization of Eq. (12) along with explicit (forward Euler) time disctretization, we obtain

$$\rho_T c_T z_T \frac{2r_j\Delta r_j}{\Delta t}\left[T_{T,j}-T_{T,j}^{old}\right]=2q''_{t,j}r_j\Delta r_j-2q''_{b,j}r_j\Delta r_j$$
$$-\left[\frac{k_T z_T(2r_j+\Delta r_j)}{\Delta r_j+\Delta r_{j+1}}\right]T_{T,j+1}^{old}-\left[\frac{k_T z_T(2r_j-\Delta r_j)}{\Delta r_j+\Delta r_{j-1}}\right]T_{T,j-1}^{old} \quad (15)$$
$$-\left[\frac{k_T z_T(2r_j+\Delta r_j)}{\Delta r_j+\Delta r_{j+1}}+\frac{k_T z_T(2r_j-\Delta r_j)}{\Delta r_j+\Delta r_{j-1}}\right]T_{T,j}^{old}$$

where the superscript "old" represents values at the previous time-step. Equation (15) represents a tridiagonal set of linear equations that can be solved readily.

Solution Algorithm

To summarize, determination of (pseudo-)temperature and heat flux in an FDTR setup requires an iterative procedure that entails the following steps:

1. The temperature of the entire solution (computational) domain is first guessed. This includes nonisothermal boundaries, such as the transducer top.
2. The BTE [Eq. (4)] is solved to determine the spectral intensity, $I_{\omega,p}$. This intensity is then post-processed to compute the incident phonon intensity, $G_{\omega,p}$, using Eq. (7). Likewise, Eq. (5) may be used to compute the heat flux at locations of interest, e.g., at boundary surfaces.
3. The computed value of $G_{\omega,p}$ is then substituted into Eq. (6) and the resulting equation is solved using a nonlinear equation solver to determine the pseudo-temperature at any given location in space and instant of time.
4. The intensities obtained from the solution of the BTE can also be used to determine the heat flux at the top surface of the substrate using Eq. (5).
5. The heat flux at the top surface of the substrate is equal to the heat flux at the bottom surface of the transducer, $q''_{b,j}$. Once this is known, Eq. (15) can be solved. Solution of Eq. (15) yields the transducer temperature.
6. With the heat flux and transducer temperature both being known, the temperature on the top of the substrate can now be computed using Eq. (14). This new temperature replaces the guess in Step 1.
7. Steps 2-6 are repeated until convergence.
8. Once convergence has been reached, the solution is marched forward in time.

RESULTS AND DISCUSSION

For the purposes of this study, the experimental data reported by Regner *et al.* [2] was used for comparison. The substrate in this experiment is a silicon block that is 525 μm thick, *i.e.*, z_S = 525 μm. The radial extent of substrate, r_S, which is not known, was assumed to be also equal to 525 μm for the numerical calculations. The transducer is a bilayer transducer with 55 nm of gold and 5 nm of chromium, resulting in z_T = 60 nm. The thermophysical properties of gold and chromium that were used for calculations are shown in Table 1. Based on the thicknesses of the gold and chromium layers, effective values of the properties of the transducer were estimated and used. These are also shown in Table 1.

Table 1: Thermophysical properties of the transducer layers.

	Transducer		
	Gold	**Chromium**	**Effective**
Density (kg/m^3)	19320	7140	18290.8
Specific heat capacity (J/kg/K)	129	450	155.7
Thermal conductivity (W/m/K)	310	93.9	266.6

For numerical calculations, a 200 x 200 nonuniform mesh with a stretching factor not exceeding 1.2 was used, as shown schematically in Fig. 4. The modulation frequency, which is an input parameter, was varied between 20 MHz and 200 MHz, with 8 different frequencies. Each sinusoidal cycle of the laser was split into 2500 time steps. This implies that a time-step size of 2 ps was used. This time step size also obeys the stability criterion of the explicit method being used here. Furthermore, it is small enough to resolve the scattering events. The nominal value of the interfacial (between the substrate and the transducer) contact conductance, G_C, was taken to be 200 MW/m^2/K, as suggested by Cahill [1], although for a different material pair. The pump and probe laser $1/e^2$ radii are inputs in the model. Here, $r_{pump} = 4.1\mu m$ and $r_{probe} = 2.8\mu m$ were used. A Gaussian laser flux profile (in r) was used for all calculations. For BTE calculations, the frequency space was discretized using 40 spectral intervals (bands) with 24 bands between 0 and $\omega_{\max,TA}$, and 16 additional bands between $\omega_{\max,TA}$ and $\omega_{\max,LA}$. The angular space was discretized using 4 azimuthal angles and 20 polar angles, resulting in a total of 80 solid angles or directions. The scattering (or relaxation) time-scales used in this study are given by Ward and Broido [24]:

$$\tau_{N,p}^{-1} = A_p^N \omega^2 T[1-\exp(-3T/\theta_D)] \quad (16a)$$

$$\tau_{U,p}^{-1} = A_p^U \omega^4 T[1-\exp(-3T/\theta_D)] \quad (16b)$$

where the subscripts N and U stand for Normal and Umklapp processes, respectively, and the subscript p stands for the polarization of the phonon, *i.e.*, either longitudinal acoustic (LA) or transverse acoustic (TA). The constants in Eq. (16) are as follows: $A_{LA}^N = 7.10\times10^{-20}$ s.rad^{-2}K^{-1}, $A_{TA}^N = 10.9\times10^{-20}$ s.rad^{-2}K^{-1}, $A_{LA}^U = 9.51\times10^{-47}$ s^3.rad^{-4}K^{-1}, $A_{TA}^U = 37.8\times10^{-47}$ s^3.rad^{-4}K^{-1}. The Mathiessen rule [9] was then used to compute the overall relaxation time-scale. Optical phonons were not considered in this study because their contributions to thermal transport in silicon have been shown to be marginal [25] except at high temperature. Dispersion relationships for silicon were used from Pop [26], which were then used to compute the phonon group velocities for all frequencies and polarizations.

*E-mail: mazumder.2@osu.edu, Fellow ASME

To bring to light the difficulty of BTE calculations for the problem at hand, a rough estimate is helpful. Since 40 bands and 80 angles are used, the calculation essentially boils down to time-marching 3200 partial differential equations on a mesh with 40,000 cells. For the 200 MHz modulation frequency, the time period for each cycle is 5×10^{-7} s. Since a time-step size of 2 ps is used, this means that the solution has to be advanced through roughly 12,500 time steps (5 cycles with 2500 time steps per cycle; see next paragraph for reasoning) before quasi-steady state is reached. Using band-based parallelization over 40 processors (same as the number of bands), the calculations require approximately 7 hours. However, for the 20 MHz modulation frequency, since the stability criterion dictates that the same time step size of 2 ps is to be used (Note: stability criterion depends on phonon speed and grid size, both of which are independent of modulation frequency), the calculation requires approximately 70 hours. An implicit time-marching scheme was also explored but was found to be computationally more expensive. Furthermore, it was found that using larger time-step size (allowable in implicit time-marching methods) negatively affected the accuracy of the computed phase.

For each simulation, the solution was advanced far enough in time such that the solution became quasi-steady. The temperature of the transducer, averaged over the probe radius (or spot), was compared against the sinusoidal pump laser flux pulse, and the phase lag was computed. This was done in two ways: (1) using the time lag from peak to peak, and (2) using the time lag from trough to trough. Figure 5 shows how the phase lag computed with these two approaches converge to a unique value as quasi-steady state is approached. It also clearly demonstrates that the phase lag converges to a unique value after about 5 pump laser cycles.

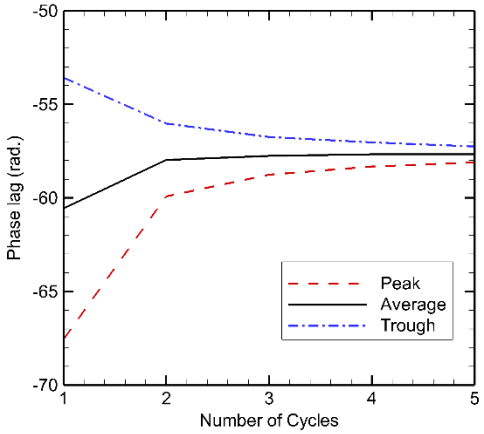

Figure 5: Convergence of phase lag using two different approaches as the solution approaches quasi-steady state.

Figure 6 shows the temporal evolution of the temperature distribution for the lowest and highest frequencies, namely 20 MHz and 200 MHz. As expected, the penetration depth, which is inversely proportional to the square root of the modulation frequency, is much smaller for the 200 MHz case.

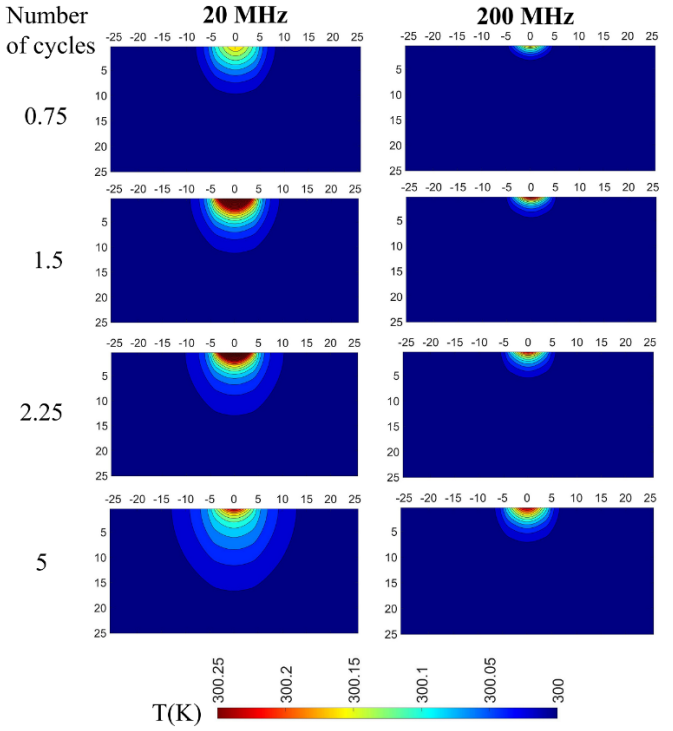

Figure 6: Temporal evolution of the temperature distribution for two different modulation frequencies. For clarity of figures, the maximum temperature is truncated at 300.25 K, even though the peak temperature at the boundary exceeds that value.

Figure 7 shows the phase lag calculated using the BTE and its comparison to the experimentally measured values. Clearly, the phase values are underpredicted by the BTE compared to the experiments, indicating that, at least with the time-scales being used in the present study (Ward and Broido [24]), the phonons have less resistance to transport (less scattering) compared to experiments. At this point, the reason for the discrepancy is not clear and further investigations will have to be undertaken to ascertain the exact cause of the discrepancy. Nonetheless, the results shown here represent the first step toward solving the multidimensional phonon BTE for an actual FDTR experimental setup in which the solution is advanced in time domain to a quasi-steady state.

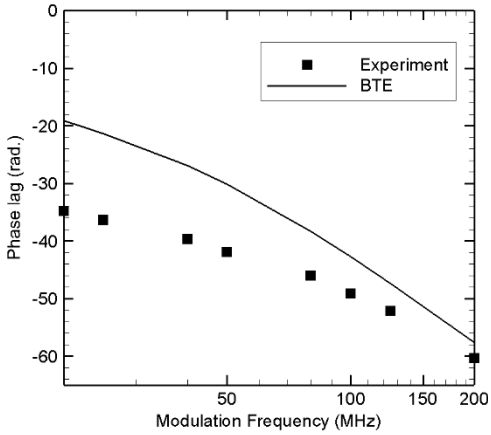

Figure 7: Comparison of phase lag computed using the phonon BTE and measured values [2].

*E-mail: mazumder.2@osu.edu, Fellow ASME

SUMMARY AND CONCLUSIONS

It is now widely accepted that the most appropriate model to extract the phonon mean free path spectrum and the size-dependent thermal conductivity from FDTR experiments is the BTE for phonons. The BTE for phonons is a seven-dimensional (six-dimensional if a spatially two-dimensional computational domain is considered) partial differential equation, making it extremely challenging to solve.

In this study, BTE computations are conducted in a two-dimensional axisymmetric geometry in cylindrical coordinates to simulate an FDTR experimental setup. The thin metallic transducer film is modeled using the Fourier law and radial conduction in the transducer is included. The governing equation in the transducer is coupled to the BTE calculations in the silicon substrate underneath using a self-consistent iterative procedure. The BTE computations are performed with a computational mesh comprised of 40,000 quadrilateral control volumes. For angular discretization, 80 solid angles (directions) are used, while for discretization of the frequency space, 40 spectral intervals (or bands) are used. For time advancement, the forward Euler (Explicit) procedure with equal time step size of 2 ps is used. Each simulation is carried out until quasi-steady state is reached. This requires approximately 5 modulation cycles of the pump laser. The convergence of the phase lag was monitored to ascertain that the solution has been advanced sufficiently in time. Computations were performed for 8 different modulation frequencies ranging between 20 MHz and 200 MHz. The longest computations required approximately 70 hours of wall clock time on a parallel system with 40 processors.

The scattering time-scales published by Ward and Briodo [24] were used in this study. With these time-scales as inputs, the phase lag computed using the BTE was found to underpredict experimentally measured values, indicating that the resistance posed by scattering to the traveling phonons is underpredicted. The exact cause for this discrepancy is not clear at this point and additional studies will have to be undertaken to pinpoint the cause. Nonetheless, the present study represents the first step toward solving the multidimensional phonon BTE for an actual FDTR experimental setup in which the solution was advanced in time domain to a quasi-steady state, as opposed to previous studies where only a single laser pulse was simulated and no attempt was made to compute the phase lag under quasi-state conditions.

ACKNOWLEDGMENTS

This research was funded, in part, by Award number 2003747 by the National Science Foundation. The Ohio Supercomputer Center (OSC) and the Department of Mechanical and Aerospace Engineering at the Ohio State University are gratefully acknowledged for providing computational resources.

REFERENCES

[1] Cahill, D. G., 2004, "Analysis of heat flow in layered structures for time domain thermo-reflectance," *Review of Scientific Instruments*, **75**, p. 5119.

[2] Regner, K.T., Sellan, D.P., Su, Z., Amon, C.H., McGaughey, A.J.H., Malen, J.A., 2013, "Broadband phonon mean free path contributions to thermal conductivity to thermal conductivity measured using frequency domain themroreflectance" *Nature Communications*, **4**: p. 1640

[3] Minnich, A.J., Johnson, J.A., Schmidt, A.J., Esfarjani, K., Dresselhaus, M.S., Nelson, K.A., and Chen, G., 2011, "Thermal Conductivity Spectroscopy Technique to Measure Phonon Mean Free Paths," *Physical Review Letters*, **107**, p. 095901

[4] Feldman, A., 1999, "Algorithm for solutions of the thermal diffusion equation in a stratified medium with a modulated heating source", *High Temperatures High Pressures*, **31**, pp. 293-298.

[5] Saurav, S. and Mazumder, S., 2022, "On the Determination of Thermal Conductivity from Frequency Domain Thermoreflectance Experiments," *Journal of Heat Transfer*, **144**, p. 013501.

[6] Koh, Y.K., and Cahill, D.G., 2007, "Frequency Dependence of the Thermal Conductivity of Semiconductor Alloys," *Physical Review B*, **76**, pp. 075207.

[7] Minnich, A.J., 2012, "Determining Phonon Mean Free Paths from Observations of Quasiballistic Thermal Transport," *Physical Review Letters*, **109**, p. 205901.

[8] Hua, C., and Minnich, A.J., 2014, "Transport Regimes in Quasiballistic Heat Conduction," *Physical Review B*, **89**, p. 094302.

[9] Tien, C.L., Majumdar, A., and Gerner, F.M., eds., 1998, *Microscale Energy Transport*, Taylor and Francis.

[10] Ma, Y., 2014, "A two-parameter nondiffusive heat conduction model for data analysis in pump-probe experiments," *Journal of Applied Physics*, **116**, p. 243505.

[11] Ramu, A.T. and Bowers, J.E., 2015, "A compact heat transfer model based on an enhanced Fourier law for analysis of frequency domain thermoreflectance experiments," *Applied Physics Letters*, **106**, p. 263102.

[12] Chen, G., 2001, "Ballistic-Diffusive Heat-Conduction Equations," *Physical Review Letters*, **86**(11), pp. 2297–2300.

[13] Mittal, A., and Mazumder, S., 2011, "Hybrid Discrete Ordinates—Spherical Harmonics Solution to the Boltzmann Transport Equation for Phonons for Non-Equilibrium Heat Conduction," *Journal of Computational Physics*, **230**(18), pp. 6977-7001.

[14] Beardo, A., Hennessy, M. G., Sendra, L., Camacho, J., Myers, T. G., Bafaluy, J., and Alvarez, F. X., "Phonon hydrodynamics in frequency-domain thermoreflectance experiments," *Physical Review B*, **101**, 075303.

[15] Mazumder, S., 2022, "Boltzmann Transport Equation Based Modeling of Phonon Heat Conduction: Progress and Challenges," in *Annual Review of Heat Transfer*, **24**, Begell House Publications; **DOI:** 10.1615/AnnualRevHeatTransfer.2022041316

[16] Peraud J-P. M. and Hadjiconstantinou N. G., 2011, "Efficient Simulation of Multidimensional Phonon Transport Using Energy-Based Variance-Reduced Monte Carlo Formulations," *Physical Review B*, **84**, p. 205331.

*E-mail: mazumder.2@osu.edu, Fellow ASME

[17] Regner, K.T., McGaughey, A.J.H., and Malen, J.A., 2014, "Analytical Interpretation of Nondiffusive Phonon Transport in Thermoreflectance Thermal Conductivity Measurements," *Physical Review B*, **90**, p. 064302.

[18] Ding, D., Chen, X., Minnich, A.J., 2014, "Radial Quasiballistic Transport in Time-Domain Thermo-Reflectance Studied Using Monte Carlo Simulations," *Applied Physics Letters*, **104**, p. 143104.

[19] Ali, S.A. and Mazumder, S., 2017, "Phonon Boltzmann Transport Equation Based Modeling of Time Domain Thermo-Reflectance Experiments," *International Journal of Heat and Mass Transfer*, **107**, pp. 607-621.

[20] Modest, M. F. and Mazumder, S., 2021, *Radiative Heat Transfer*, Fourth Edition, New York: Academic Press.

[21] Majumdar, A., 1993, "Microscale Heat Transfer in Dielectric Thin Films," *Journal of Heat Transfer*, **115**, pp. 7-16.

[22] Mazumder, S. and Majumdar, A., 2001, "Monte Carlo Study of Phonon Transport in Solid Thin Films Including Dispersion and Polarization," *Journal of Heat Transfer*, **123**, pp. 749-759.

[23] Mazumder, S., 2016, *Numerical Methods for Partial Differential Equations: Finite Difference and Finite Volume Methods*, First Edition, New York: Academic Press.

[24] Ward, A., and Broido, D.A., 2010, "Intrinsic phonon relaxation times from first principles studies of the thermal conductivities of Si and Ge," *Physical Review B*, **81**(8), p. 085205.

[25] Mittal, A., and Mazumder, S., 2010, "Monte Carlo Study of Phonon Heat Conduction in Silicon Thin Films Including Contributions of Optical Phonons," *Journal of Heat Transfer*, **132**, p. 052402.

[26] Pop, E., 2004, "Self-heating and scaling of thin body transistors" *PhD. Dissertation*, *Department of Electrical Engineering*, Stanford University.

*E-mail: mazumder.2@osu.edu, Fellow ASME